Estimation of kinematic source parameters and frequency independent shear wave quality factor around Bushehr

Hoda Mahmoodi[1], Habib Rahimi[2*], and Behzad Maleki[1]

[1]*M. Sc., Institute of Geophysics, University of Tehran, Tehran, Iran*
[2]*Assistant Professor, Institute of Geophysics, University of Tehran, Tehran, Iran*

(Received: 25 December 2017, Accepted: 02 February 2019)

Abstract

In this paper, the shear wave quality factor and source parameters in the near field are estimated by analyzing the acceleration data in Zagros region. Accelerograms recorded by Building and Houses Research Center strong ground motion network have been used. The data have been considered with the magnitude of 4.7 to 6.3 collected from 1999 to 2014. In this approach, the theoretical S-wave displacement spectra conditioned by frequency independent Q was fitted with the observed displacement spectra. The source spectrum of an earthquake can be approximated by the omega-square ω^2 model, which has ω^2 decay for frequencies higher than the corner frequency. By following the mentioned approach, corner frequency, scalar moment, moment magnitude and frequency independent Q for each accelerogram were computed simultaneously, and the estimated error was given in the root-mean-square sense over the frequency range of interest. In this study, the generalized inversion method is used to estimate various source parameters as listed below. Thereby, it is estimated that the seismic moment range from 2.89E+23 to 1.21E+26 dyne-cm, average fault slip from 22 to 152 cm and average stress drop from 6 to 136 bars. The path average value Q are of the order Q=151-537.

Keywords: Quality factor, Source parameters, Inversion method, Source spectrum

[*]Corresponding author: rahimih@ut.ac.ir

1 Introduction

The main objective of this study is to determine the kinematic source parameters and the shear wave quality factor. Kinematics is a branch of classical mechanics that describes the motion of points, bodies, and systems of bodies without considering the forces that caused the motion. The study of the earthquake source rupture process through the modeling of the observed seismic radiation, in general, is done by adopting a kinematic approach to describe the seismic source (Beroza and Spudich, 1988; Zhang et al., 2003). The kinematic description of the earthquake source has the advantage of using a limited number of parameters to characterize the source, such as fault size, the final slip distribution on the fault, the rupture velocity, and the slip duration (rise time).

We chose to study the attenuation of S-waves based on the fact that S-waves are more destructive compared to the P waves. The amplitudes of shear waves are about five times larger compared to the amplitudes of longitudinal waves and their periods are longer by at least a factor of 3. These facts arise from differences in wave propagation velocities and the related differences in the corner frequencies of the P - and S - wave source spectra. Thus, the study of the attenuation of shear waves has important engineering implications.

In this study, the strong motions were used for analyzing the source parameters of 14 occurred events since 1990. In this study, the source spectrum has been estimated based on the omega-square model (Brune, 1970), which has ω^2 decay for frequencies higher than the corner frequency. Acceleration spectrum is one of the most direct and common data used to describe the frequency content of strong ground earthquake shaking (Hudson, 1962).

The source displacement spectrum can be approximated from a displacement record after correcting with diminution function, which accounts for geometrical spreading and anelastic attenuation (Boore and Atkinson, 1987; Joshi, 2006a, 2006b; Zafarani et al., 2013). The seismic hazard related to the future large earthquakes will be achieved by specifying anelastic attenuation characteristic of seismic waves released during an earthquake. The anelastic attenuations of seismic wave in any area described by a dimensionless quantity called quality factor Q (Knopoff, 1964; Mahood, 2014). Up to now, a few research have been devoted to the investigation of the issue of attenuation characteristics of the Iranian crust, on which some researchers have worked such as Nuthii (1980), Mitchel (1995), and Rahimi and Hamzehloo (2008). In the present work, the generalized inversion method was used to determine source parameters and quality factor of shear waves based on the proposed techniques of Fletcher (1995) and Joshi (2006a, 2006b). The acceleration data recorded by Building and Housing Research Center (BHRC) strong ground motion network was collected to reach our goals. In this study, two main goals are attempted to be obtained: i) to estimate the kinematic source parameters by using the acceleration data; ii) to estimate the frequency independent shear wave quality factor in the Bushehr region.

2 Tectonic setting

Alpine-Himalayan seismic belt is recognized as one of the seismically active areas of the world. The Iranian plateau, situated on this belt, has experienced several major and destructive earthquakes in the recent past. Deformation and seismicity in this region is mainly due to the continental shortening between Eurasian and Arabian

plates. Iranian plateau is principally divided into five major geological units-based on remarkable tectonic history, magmatic events or sedimentary features (Nabavi, 1976). These units are Zagros, Sanandaj-Sirjan, Central Iran, East and South-East zones and Alborz, each of which is subdivided into a number of sub-units with specific characteristics. The study area is located in Zagros region shown in Figure 1. The deformation in the Iranian plateau is related to the continuous convergent movement between Arabian plate to the southwest and Turan platform to the northeast with the north-northeast drift of Afro-Arabian plate against Eurasia. Iran is one of the seismically active regions of the world in which destructive earthquakes occur almost every year, causing costly losses in human life and widespread damages. The Zagros Fold-Thrust Belt as a part of the Alpine-Himalayan orogenic belt is one of the youngest and most active collision zones on the earth (Snyder and Barazangi, 1986) which extends about 1500 km from Tarus Mountains in southeastern Turkey to the fault in the east of Strait of Hormoz in the Persian Gulf. Highly seismic regions of Alborz-Azarbayjan covered the north and the northwest of Iran, which constitute a part of the northern limit of Alpine-Himalayan orogenic belt. Alborz-Azarbayjan major province is a significant belt of seismicity that covers the northwestern Iran and southern of the Caspian Sea. Continental collision zone in the northeast, Koppeh-Dagh, constituting a part of the northern limit of the Alpine-Himalayan mountain belt and its formation is the result of Arabian-Eurasia convergence moments. It is homologous to the Zagros, which forms the corresponding southeastern limit of the belt (Tchalenko and Berberian, 1975). Ocean continental subduction zone in southeast Iran, Makran, region of southeastern Iran and southern Pakistan is a 1000 km section of the Eurasian-Arabian plate boundary extending from Strait of Hormoz in Iran to the mouth of the Indus River in Pakistan, where consumption of oceanic crust has occurred continuously since the Early Cretaceous along a north-dipping subduction zone (e.g., Page et al., 1979; Byrne et al., 1992). The covered area in this study is situated in the Zagros zone in western and southwestern Iran at the eastern edge of the Persian Gulf. Figure 1 shows the location of Zagros Mountains.

The work presented here is complicated information on earthquakes that occurred 300 km far from Bushehr province, as a result, the study area is situated in the Simply Folded Belt of the Zagros Mountains in South-Western of Iran. It seems that earthquakes in the Zagros belt are limited to the upper continental crust with depths less than 20 km with average magnitude less than 6 (Jackson and Fitch, 1981). The largest earthquake in recent decade has occurred in this region was Kaki earthquake with M_w=6.2. The distribution of historical earthquakes around Bushehr is depicted in Figure 2, showing that the area has experienced more than five large earthquakes with magnitudes greater than 6 from 4^{th} B.C to 1900 (Ambraseys and Melville, 1982; Ambraseys, 1988).

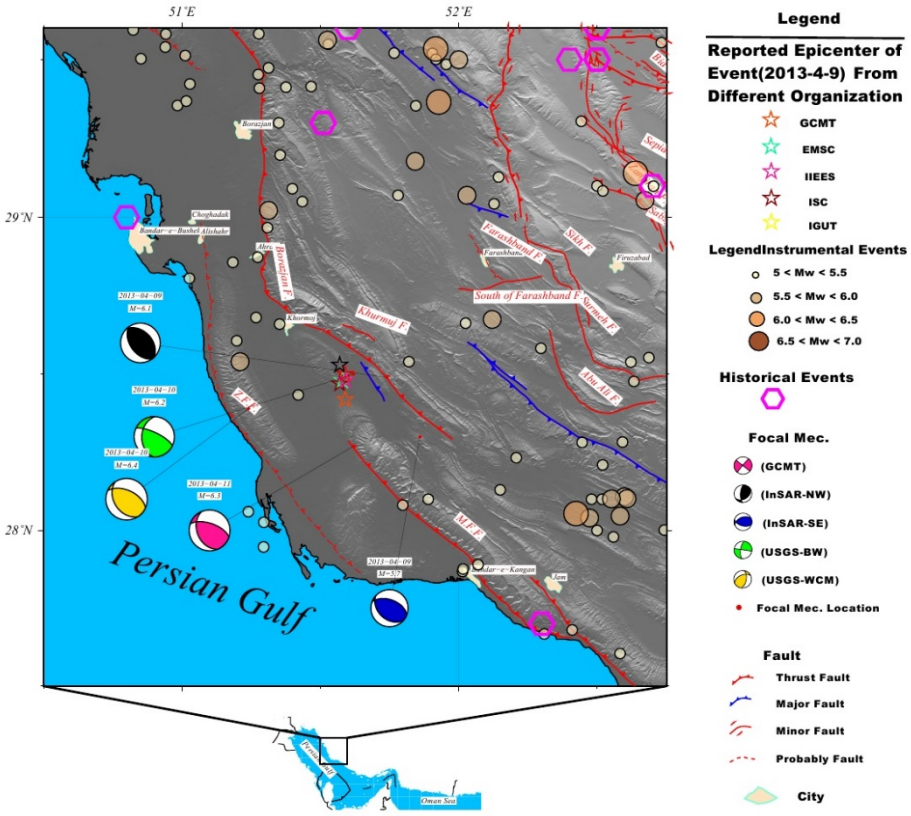

Figure 1. Tectonic and Geomorphological map of the SE Zagros (Mohammadi and Bayrak, 2015)

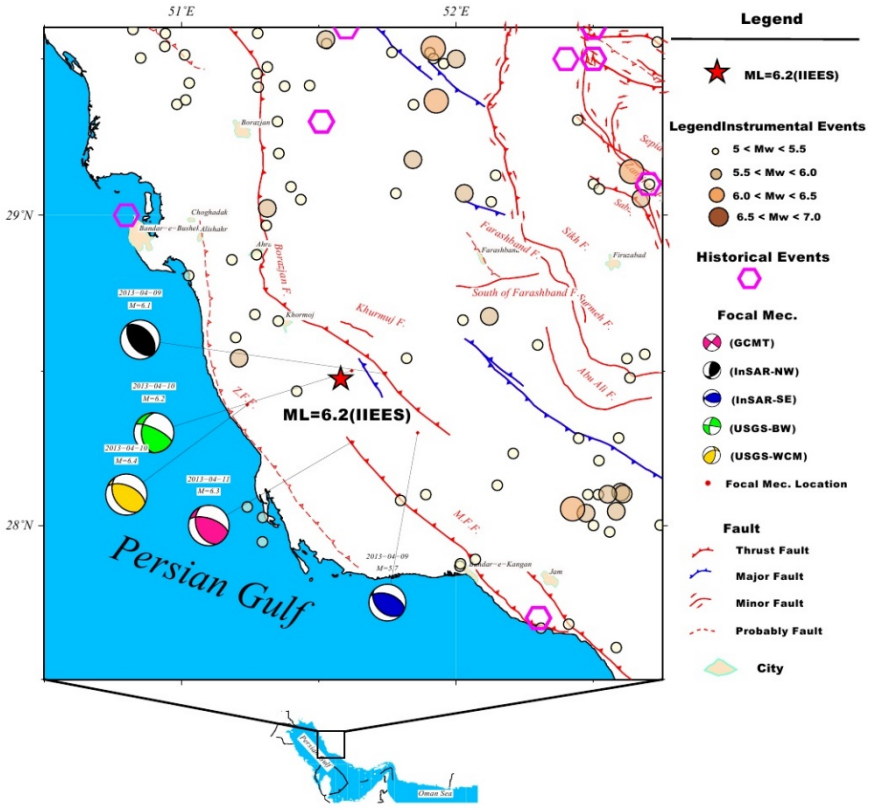

Figure 2. Historical and instrumental earthquake around Bushehr city 1900-2013.

3 Data and analysis

The strong motion data recorded by BHRC network are used in this study. All accelerographs are the Digital SSA-2 type with the threshold of 10 gals at the sampling rate of 200 samples, recording the signals from three components. This configuration yields a flat acceleration response between the frequencies of 0.01 to 50. In the study area more than 200 strong motion time series were recorded by BHRC network during 1999 to 2014; however, 121 accelerograms which have a good signal to noise ratio were selected to estimate the source parameters and shear wave quality factor (Figure 3).

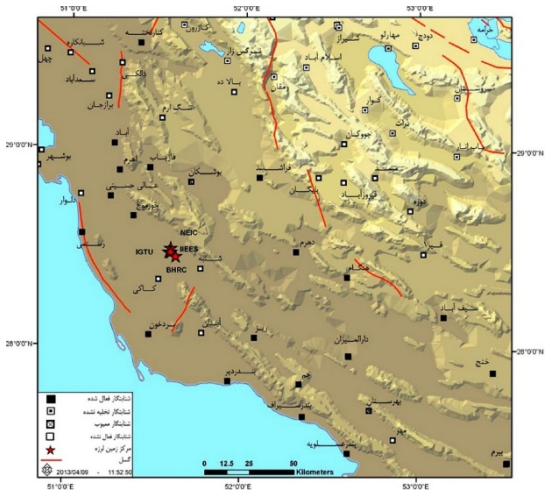

Figure 3. Map of BHRC stations used in this study.

To analyze the acceleration records and after instrumental correction, all the recorded waveforms was corrected for drift and baseline by following the algorithm developed by Boore and Boomer (2005). In the second step, two horizontal components of acceleration were low-pass filtered, with cut-off frequency at 25 Hz, and then vectorized. The resulting component, a(t), is transverse to the direction of propagation of the earthquake waves, and a time window containing the direct SH wave was selected from the accelerograms by using Kinoshita (1994) algorithm. As an example, the procedure applied to select the shear wave window is shown in Figure 4. For this aim, each acceleration record was corrected for drift and baseline. Next, the data of two horizontal components were rotated to determine the transverse and radial component of ground motion along the source-receiver azimuth direction. The time series, $x(n)$ of both components (n is the sample number) were processed in the following manner. First, $x(n)$ was band pass filtered to obtain, say, $b(n)$. Following Kinoshita (1994), for the selection of *S*-wave section in $x(n)$, an acceleration envelope $(n) = [b^2(n) + H^2 b(n)]^{\frac{1}{2}}$, was computed, where Hb(n) is the Hilbert transform of band pass-filtered time series $b(n)$. Typically, the value of e(n) increases with the arrival of the S-wave phase and then abates with its passage. Finally, the end of shear wave was calculated from the cumulative root mean square function $c(n) = [l^{-1} \sum_{n=1}^{n=l} e(n)^2]^{\frac{1}{2}}$ from e(n). The end time, T_e of the S-wave window was assigned as the point on the time axis where c(n) starts to decrease. The onset of s-wave, T_s, is picked by eyes. The displacement and acceleration spectra estimated using Fast Fourier Transform, after applying a 10% cosine taper to both ends of the data method by measuring the maximum peak-to-peak amplitudes. Mean values of half of the peak-to-peak amplitudes in two horizontal components provide the spectral amplitudes in each frequency band. The site conditions of most BHRC stations are unknown. Since the SH waves are slightly affected by the crustal heterogeneities (Haskell, 1960; Kumar et al., 2005), as well as the correction for mode conversion at the surface is not needed, the scattering effects, as well as the site amplification effects, which usually are present in limited frequency range, are neglected.

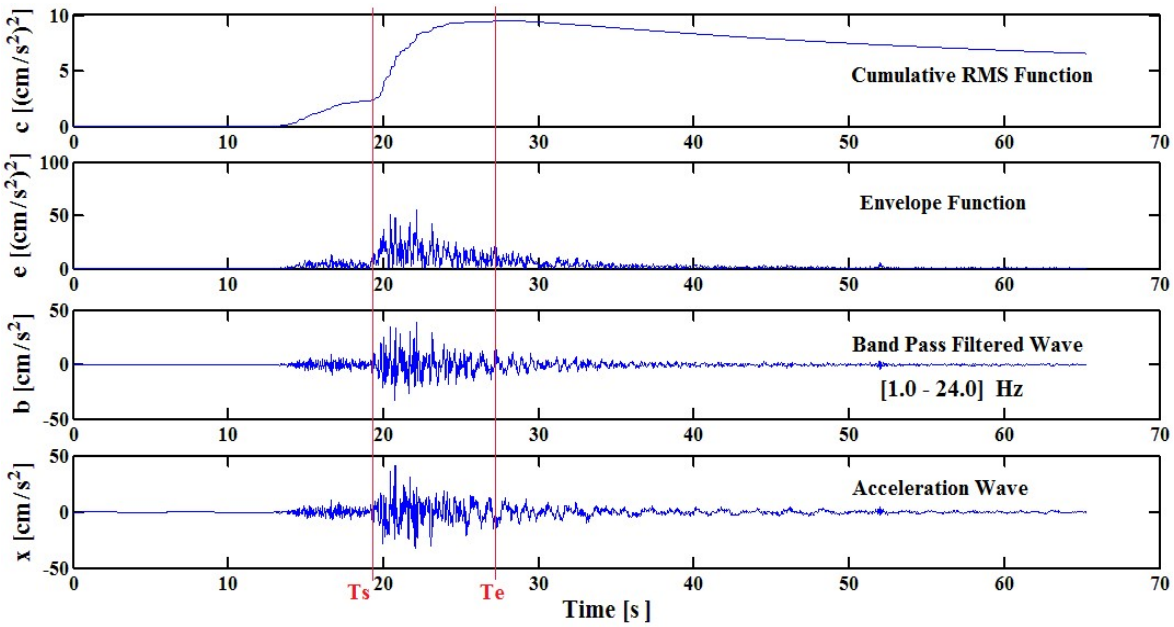

Figure 4. An example of Kinoshita algorithm to determine a time window containing the SH window. Ts and Te stand for the estimated onset and end times of the direct S wave.

4 Methodology

In this step, we estimated M_0, corner frequency and frequency-independent Q from a generalized inversion method for each selected accelerogram. The displacement spectrum of shear waves at distance R due to an earthquake of seismic moment M_0 can be given as (Boore and Atkinson, 1987; Joshi, 2006a, 2006b):

$$D(f) = CM_0S(f)R_s(f)\left[e^{-\pi ft} \quad G(R)\right] \qquad (1)$$

In the above equation, the function G(R) represents the geometrical attenuation term and is taken to be equal to 1/R for R<100 km and equal to 1/(10 √R) for R>100 km (Singh et al., 1999). As most of the data used in this work are within R>100 km, G(R) used as 1/ (10 √R) in this present work. In this expression, C is constant and given as (Boore, 1983):

$$C = \frac{R_{\theta\emptyset}F_SPRTITN}{4\pi\rho^{\ 3}} \qquad (2)$$

where $R_{\theta\emptyset}$ is the radiation pattern; F_S is the amplification due to the free surface; - PRTITN is the reduction factor that accounts for partitioning of energy into two horizontal components, and ρ and β are dense and the shear wave velocity, respectively. $R_s(f)$ denote the site amplification factor and the S(f) defines the source spectrum of the earthquake under consideration. This study follows the displacement source spectrum explained by Brune (1970) and therefore consider,

$$S(f) = \frac{1}{1+\left(\frac{f}{f_c}\right)^2} \qquad (3)$$

where f_c is the corner frequency, and $f_c = 2.34\,\beta/2\,\pi r_0$ with r_0 denoting the radius of the equivalent earthquake in Equation (1) explains the decay of the displacement spectrum with distance due to the anelastic attenuation and scattering. The parameter $t \ = R/Q\beta$ is defined as attenuation time. Equation (1) is linearized by taking natural logarithm:

$$lnD(f) = lnC + lnM_0 + lnS(f) - \pi t \quad f + lnG(R) + lnR_s(f) \qquad (4)$$

where t and M_0 are unknown parameters. The value of f_c is chosen in an iterative manner and therefore, two

unknowns, Q and M_0, can be obtained from the inversion by minimizing in the least-square sense. The least square inversion minimizes:

$$X^2=\sum[D_S(f)-S(f)]^2 \quad (5)$$

where $S(f)$ is the source displacement spectrum as suggested by Brune (1970). In order to analyze, Equation (4) is rearranged based on known and unknown parameters on different sides, in the following form:

$$lnM_0-\pi t\ \ f=lnD(f)-lnC-lnS(f)+lnG(R)-lnR_s(f) \quad (6)$$

This leads to the following set of equations for frequencies f_i , i=1, 2, and 3…n, where n is the total number of displacement spectrum in the acceleration records:

$$lnM_0-\pi f_i t\ \ =K(f_i) \quad (7)$$

With

$$K(f_i)=lnD(f_i)-lnC-lnS(f_i)+lnG(R) \quad (8)$$

In matrix from Equation (7) can be written as:

$$\begin{bmatrix}1 & -\pi f_1\\ 1 & -\pi f_2\\ . & .\\ . & .\\ 1 & -\pi f_n\end{bmatrix}\begin{bmatrix}lnM_0\\ t\end{bmatrix}=\begin{bmatrix}K(f_1)\\ K(f_2)\\ K(f_3)\\ .\\ .\\ .\\ K(f_n)\end{bmatrix} \quad (9)$$

It provides a basic statement of the following problem in which the model parameters and the data are in some way related to each other (Menke, 1984):

$$Gm=d \quad (10)$$

Here, G represents the rectangular matrix, m the model matrix, and d the data matrix. Inversion of G gives the following model matrix, m, using Newton's method for least squares case:

$$m=(G^TG)^{-1}G^Td \quad (11)$$

This inversion is prone to a problem if G^TG is close to beginning singular, and in such a case, singular value decomposition (SVD) is used to solve for m (Press et al., 1992). In this equation, the G matrix is decomposed U_p, V_p and A_p matrices as (Fletcher, 1995; Joshi, 2006a, 2006b):

$$G^{-1}=V_PA_PU_P^T \quad (12)$$

where $U_P, V_P,$ and A_P have nonzero eigenvectors and eigenvalues.

The determined corner frequency and seismic moment for each accelerogram are used to compute the frequency-dependent Q. The frequency-dependent Q is obtained by the least square method. In this method, the corrected observed displacement from source effect was fitted with path term to compute frequency- dependent shear wave quality factor. Accordingly, the frequency-dependent Q has computed by dividing source terms:

$$\frac{Q_s(f)}{-\pi fR}=\frac{}{\beta\{lnD(f)-lnC-lnS(f)-lnM_0+lnG(R)\}} \quad (13)$$

where $Q_s(f)=Q_0f^{\alpha}$ for linearizing this equation, we tacked natural logarithm on each side of Equation (13).

$$lnQ_0+\alpha lnf=ln\left\langle\frac{-\pi fR}{\beta\{lnD(f)-lnC-lnS(f)-lnM_0+lnG(R)\}}\right\rangle \quad (14)$$

From Equation (14) and least squares technique, Q_0 and α are determined.

5 Results and Discussion

In this study using acceleration data, corner frequency, moment magnitude and frequency independent Q for each record was computed simultaneously. The analysis of the strong motion acceleration data has been provided using the model of Brune (1970). In the Brune model, the specifications of frequency related to the corner frequency, furthermore corner frequency is related to the source size, as

based on the comparison of the root-mean-square (RMS) error. For example, the results of the Brune's model are shown in Figures 5, 6 and 7. In the right hand of these figures, as an example of step 1 algorithm, the displacement spectra of recorded waveform and the fitted Brune (1970) source model is shown. In the left hand of these figures, the error value between theoretical and observed models for M_W, f_c and path average Q parameters from Equation (5) are shown. In Table 1, the mean value of the best estimates of fc is given. The best approximation is varied from 0.21 Hz to 1.80 Hz. The dislocation source radius, r can be derived from relation $r_0 = \frac{2.34\ \beta}{2\pi f_c}$ where β=3.5 km/s, and f_c is corner frequency. The mean value of source radius for each earthquake is calculated and given in Table 1. Seismic moment is one of the most important parameters that has been estimated from a generalized inversion method for each accelerogram. The average seismic moment of each event is given in Table 1. For estimation of moment magnitude, Hanks and Kanamori (1979) relation is used as follows:

$$M_w = (2/3)logM_0 - 10.7 \quad (15)$$

In Table 1, the mean value of moment magnitude (dyn-cm) for each event is given. In the present work, to calculate the stress drop, a relation from Brune is used (1971):

$$\Delta\sigma = (7/16)\frac{M_0}{r^3} \quad (16)$$

The average slip, calculated from $\Delta u = \frac{M_0}{\mu\pi r^2}$ in which, μ=3.5× 10^{11} dyne/cm^3 estimated from $\mu=\rho\beta^2$. The Brune's model assumes a circular dislocation and bidirectional propagation, given source duration as $T_d = r/v_r$, where v_r is the rupture velocity. Assuming that $v_r = 0.85\beta$ gives an estimation of the source duration $T_d = 2r/v_r$ which has a good agreement with the relation $T_d = 1/f_c$ used by Hanks and McGuire (1981) that gives 0.55 to 4.7 s as an estimation of the source duration. In this step, the average value of a shear wave quality factor in the frequency range of 0.1-25 Hz for each acceleration data has been calculated.

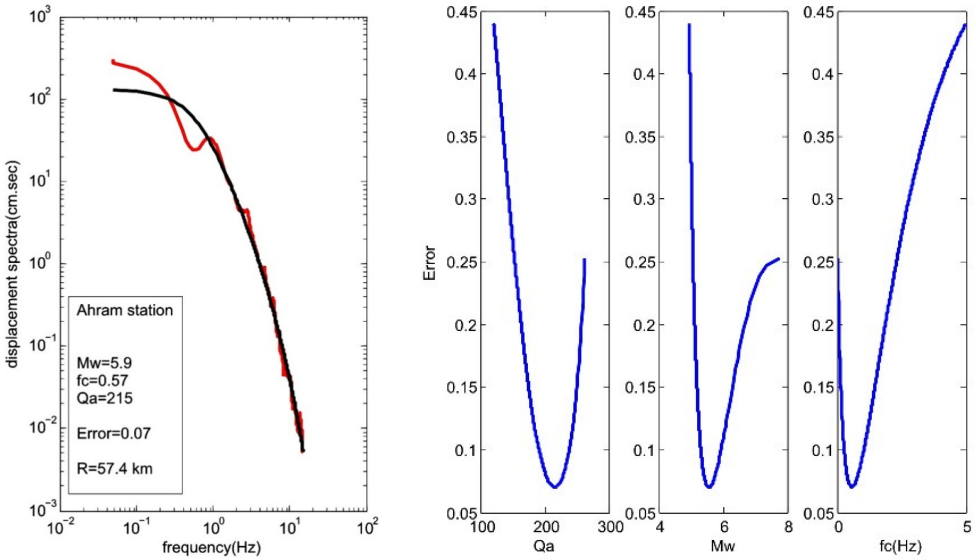

Figure 5. Example of algorithm in Ahram station is shown. The displacement spectra and the fitted Brune (1970) source model in the left hand and in the right hand, the error value between theoretical and observed models for M_w and path average Q parameters is shown.

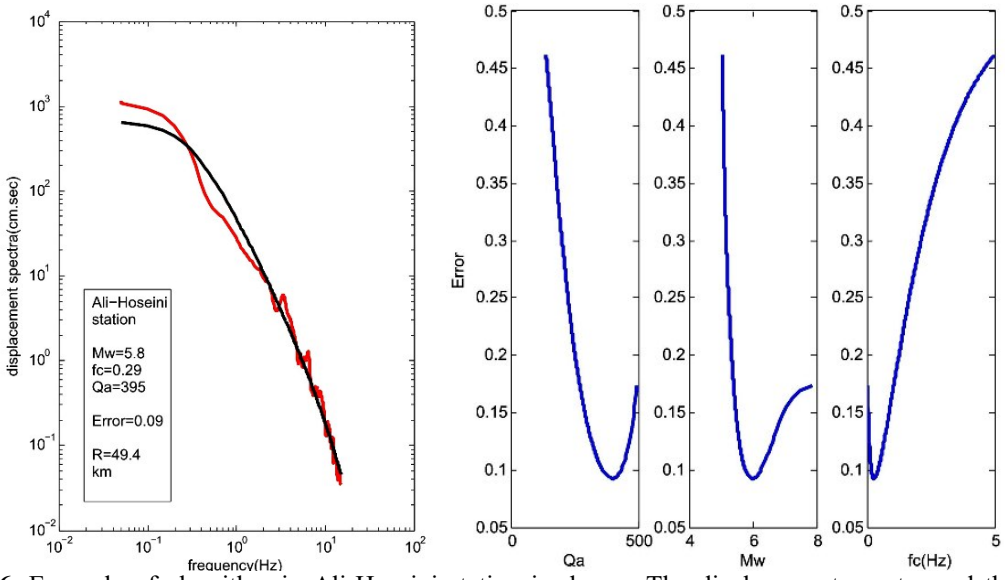

Figure 6. Example of algorithm in Ali-Hoseini station is shown. The displacement spectra and the fitted Brune (1970) source model in the left hand and in the right hand the error value between theoretical and observed models for M_w and path average Q parameters is shown.

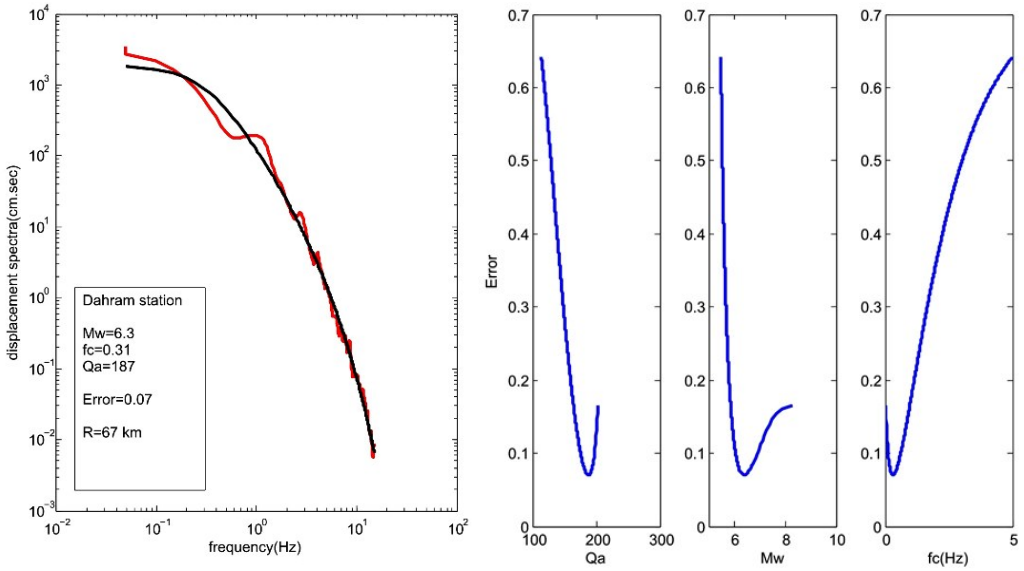

Figure 7. Example of algorithm in Dahram station is shown. The displacement spectra and the fitted Brune (1970) source model in the left hand and in the right hand the error value between theoretical and observed models for M_w and path average Q parameters is shown.

Shear wave quality factor, Q, is obtained as the solution that gives the best overall fit to the data over the spectrum in the frequency band 0.1 to 25 Hz. The mean value of Q is estimated for each event in Table 1. Figure 8 shows the path average shear wave quality factor changes with the hypocentral distance that follows Qa= 1.48R+164 in which R is hypocentral distance in Km. This figure shows the shear wave quality factor Q increase with increasing hypocentral distance. Generally, the Q value decreasing with an increase in crust depth is expected. As the rays penetrate to the greater depth in propagating longer distances, the attenuation dependence is expected at the epicentral distances. Consequently, the amounts of the attenuation shows which sites have a deeper depth, the shear wave quality factor Q is more than the others.

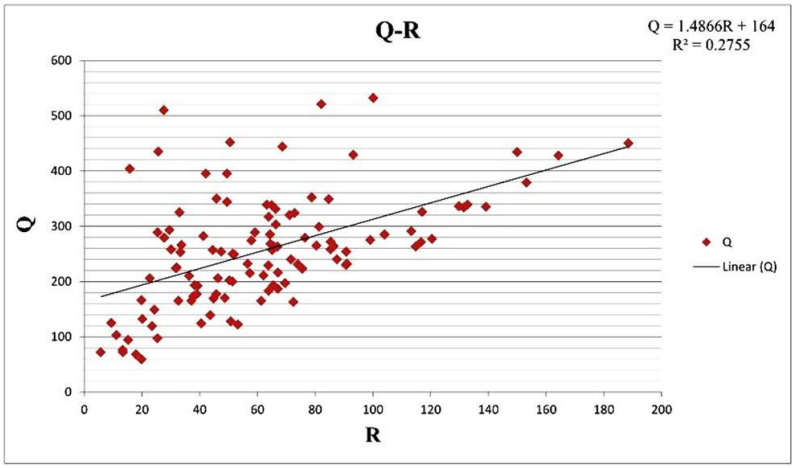

Figure 8. This figure shows the variation of path average shear wave quality factor with hypocentral distance.

Table 1. The mean and standard deviation of estimated parameters.

Date	F_C (Hz)	Mean M_0 Dyne-Cm M0*(E+25)	STD of M_0 Dyne-Cm M0*(E+16)	M_w (for each earthquake)	M_w (ISC)	Mean Path Average Q	Mean $\Delta\sigma$ bars	Mean Δu (cm)	Number of Station
1999.05.06	0.21±0.04	1.5849	2.2387	6.1±0.2	6.2	285±23	29	38.2	20
2000.05.03	0.66±0.05	0.0355	3.1623	5±0.3	5	249±33	20	8.40	5
2000.06.23	0.81±0.03	0.0355	1.5849	5±0.1	4.9	537±27	37	12.7	6
2003.07.10	0.71±0.04	0.1995	2.2387	5.5±0.2	5.6	183±18	141	54.9	5
2005.08.09	1.77±0.06	0.0178	4.4668	4.8±0.4	4.8	368±27	194	30.4	7
2010.05.14	0.76±0.05	0.0501	2.2387	5.1±0.2	5	253±18	43	15.8	7
2010.07.20	0.30±0.07	0.5623	2.2387	5.8±0.2	5.8	288±20	30	27.6	6
2010.09.27	0.69±0.06	0.2818	3.1623	5.6±0.3	5.6	282±18	183	73.3	16
2011.01.05	1.08±0.08	0.0501	2.2387	5.1±0.2	5.1	470±25	125	31.9	5
2013.04.09	0.29±0.03	2.2387	1.5849	6.2±0.1	6.3	393±26	108	102.8	16
2013.04.10 (01.58)	0.41±0.06	0.2818	1.5849	5.6±0.1	5.6	289±27	38	25.9	6
2013.04.10 (08:00)	1.80±0.05	0.0501	3.1623	5.1±0.3	5.2	151±26	577	88.7	6
2013.11.28	0.55±0.05	0.2818	2.2387	5.6±0.2	5.6	343±34	93	46.6	10
2014.04.16	0.87±0.06	0.0178	2.2387	4.8±0.2	4.7	213±26	23	7.4	5

6 Conclusion

In present work, the source parameters and shear wave quality factor Q have been estimated on Zagros zone around Bushehr province. To analyze these parameters used the acceleration data recorded by the Building and Houses Research Center (BHRC) from 1999 to 2014. This study used inversion method to obtain the M0, moment magnitude, corner frequency, and frequency independent Q for each station. In this method, the theoretical S-wave displacement spectra, conditioned by frequency-independent Q was fitted with the observed displacement spectra. In conclusion, by estimating these parameters, we can evaluate seismic hazard in this region, in addition, simulation ground motion in the Zagros to decreasing the fatalities. In this work, the average values of a seismic moment is approximated from (2.89E+23 to 1.21E+26 dyne-cm) corner frequency (0.21 t0 1.80 Hz), fault slip from (22.84 to 151.57 cm), stress drop (6.27 to 136 bars) and moment magnitude from 4.7 to 6.2. This finding will be useful in seismic hazard assessment and simulated strong ground motion. The mean value of the path average Q for 14 events from 151 to 537 is also obtained and the equation

Qa = 1.48R+164 which shows the variation of path average quality factor with epicentral distance is acquired.

References

Ambraseys, N. N., 1988, Engineering seismology: part II. Earthquake Engineering and Structural Dynamics, **17**(1), 51-105.

Ambraseys, N. N., and Melville, C. P., 1982, A History of Persian Earthquakes: Cambridge University Press, London, 219 pp.

Beroza, G. C., and Spudich, P., 1988, Linearized inversion for fault rupture behaviour: application to the 1984 Morgan Hill, California, earthquake: Journal of Geophysical Research, **93**, 6275–6296.

Boore, D. M., 1983, Stochastic simulation of high-frequency ground motions based on seismological models of the radiated spectra: Bulletin of the Seismological Society of America, **73**, 1865-1894.

Boore, D. M., and Atkinson, G. M., 1987, Stochastic prediction of ground motion and spectral response parameters at hard-rock sites in eastern North America: Bulletin of the Seismological Society of America, **77**(2), 440-467.

Boore, D. M., and Bommer, J. J., 2005, Processing of strong-motion accelerograms, needs, options and consequences: Soil Dynamics and Earthquake Engineering, **25**, 93-115.

Brune, J. N., 1970, Tectonic stress and the spectra of seismic shear waves from earthquakes: Journal of geophysical research, **75**, 4997-5009.

Brune, J. N., 1971, Correction: Journal of Geophysical Research, **76**, 5002.

Byrne, D. E., Sykes, L. R., and Davis, D. M., 1992, Great thrust earthquakes and aseismic slip along the plate boundary of the Makran subduction zone: Journal of Geophysical Research, Solid Earth, **97**(B1), 449-478.

Fletcher, J. B., 1995, Source parameters and crustal Q for four earthquakes in South Carolina: Seismological Research Letters, **66**, 44-61.

Hanks, T. C., and Kanamori, H., 1979, A moment magnitude scale: Journal of Geophysical Research., **84**, 2348-2350.

Hanks, T. C., and McGuire, R. K., 1981, The character of high-frequency strong ground motion: Bulletin of the Seismological Society of America, **71**, 2071-2095.

Haskell, N. A., 1960, Crustal reflection of plane SH waves: Journal of Geophysical Research, 65, 4147-4150.

Hudson, D. E., 1962, Some problems in the application of spectrum techniques to strong-motion earthquake analysis: Bulletin of the Seismological Society of America, **52**, 417-430.

Jackson, J., and Fitch, T., 1981, Basement faulting and the focal depths of the larger earthquakes in the Zagros Mountains (Iran): Geophysical Journal International, **64**, 561-586.

Joshi, A., 2006a, Use of acceleration spectra for determining the frequency-dependent attenuation coefficient and source parameters: Bulletin of the Seismological Society of America, **96**, 2165-2180.

Joshi, A., 2006b, Analysis of strong motion data of the Uttarkashi earthquake of 20th October 1991 and the Chamoli earthquake of 28th March 1999 for determining the mid crustal Q value and source parameters: ISET Journal of Earthquake Technology, **43**, 11-29.

Kinoshita, S., 1994, Frequency-dependent attenuation of shear waves in the crust of the southern Kanto area, Japan: Bulletin of the Seismological Society of America, **84**(5), 1387-1396.

Knopoff, L., 1964, Department of Physics and Institute of Geophysics and Planetary Physics. University of California, Los Angeles: Reviews of Geophysics, **2**(4), 625-660.

Kumar, D., Sarkar, I., Sriram, V. and Khattri, K. N., 2005, Estimation of the source parameters of the Himalaya earthquake of October 19, 1991, average effective shear wave attenuation parameter and local site effects from accelerograms: Tectonophysics, **407**, 1-24.

Mahood, M., 2014, Attenuation of high-frequency seismic waves in Eastern Iran: Pure and Applied Geophysics, **171**, 2225-2240.

Menke, W., 1984, Geophysical Data Analysis: Discrete Inverse Theory Academic, New York.

Mitchell, B. J., 1995, Anelastic structure and evolution of the continental crust and upper mantle from seismic surface wave attenuation: Reviews of Geophysics, **33**(4), 441-462.

Bayrak, Y., and Mohammadi, H., 2015, The Mw 6.3 Shonbeh (Bushehr) mainshock, and its aftershock sequence, Tectonic implications and seismicity triggering: Eastern Anatolian Journal of Science, **1**(1), 43-56.

Nabavi, M. H., 1976, An introduction to the geology of Iran: Geological Survey of Iran, in Farsi, 110 pp.

Nuttli, O. W., 1980, The excitation and attenuation of seismic crustal phases in Iran: Bulletin of the Seismological Society of America, **70**(2), 469-485.

Page, W. D., Alt, J. N., Gluff L. S., and Plafker., G., 1979, Evidence for the recurrence of large magnitude earthquake along the Makran coast of Iran and Pakistan: Tectonophysics, **52**, 533-542.

Press, W. H., Flannery, B. P., Teukolsky, S. A., and Vetterling, W. T., 1992, Singular value decomposition, §2.6 in numerical recipes in FORTRAN, The Art of Scientific Computing, 2nd ed. Cambridge, England: Cambridge University Press, 51-63

Rahimi, H., and Hamzehloo, H., 2008, Lapse time and frequency-dependent attenuation of coda waves in the Zagros continental collision zone in Southwestern Iran: Journal of Geophysics and Engineering, **5**(2), 173.

Singh, S. K., Ordaz, M., Dattatrayam, R. S., and Gupta, H. K., 1999, A spectral analysis of the 21 May 1997, Jabalpur, India, earthquake (Mw = 5.8) and estimation of ground motion from future earthquakes in the Indian shield region: Bulletin of the Seismological Society of America, **89**(6), 1620-1630.

Snyder, D. B., and Barazangi, M., 1986, Deep crustal structure and flexure of the Arabian plate beneath the Zagros collisional mountain belt as inferred from gravity observations: Tectonics, **5**(3), 361-373.

Tchalenko, J. S., and Berberian, M., 1975, Dasht-e Bayaz fault, Iran, earthquake and earlier related structures in bed rock: Geological Society of America Bulletin, **86**(5), 703-709.

Zafarani, H., Hassani, B., and Ansari, A., 2012, Estimation of earthquake parameters in the Alborz seismic zone, Iran using generalized inversion method: Soil Dynamics and Earthquake Engineering, **42**, 197-218.

Zhang W., T. Iwata, K. Irikura, H. Sekiguchi, and M. Bouchon (2003), Heterogeneous distribution of the dynamic source parameters of the 1999 Chi-Chi, Taiwan, earthquake, Journal of Geophysical Research, 108(B5), 2232, doi: 10.1029/2002JB001889.